

Communication

The Shell Matters: Self-Organized CdS-ZnS/MnS-Core-Shell—Porphyrin-Polymer Nano-Assemblies for Photocatalysis

Maximilian Wagner and Franziska Gröhn *

Department of Chemistry and Pharmacy & Interdisciplinary Center for Molecular Materials, Bavarian Polymer Institute, Friedrich-Alexander-Universität Erlangen-Nürnberg Egerlandstraße 3, 91058 Erlangen, Germany

* Correspondence: franziska.groehn@fau.de

Abstract: A facile synthesis of catalytically tunable core-shell CdS-Zn_xMn_{1-x}S-nanoparticles in conjunction with poly(acrylic acid) (PAA) and porphyrin in an aqueous solution is described in the following: The shell composition of the inorganic nanoparticles is varied to tune the optical properties and to optimize the catalytic activity. Further, the tetravalent cationic 5,10,15,20-tetrakis(4-trimethylammonio)phenyl porphyrin (TAPP) fulfills a triple functionality in the catalyst: as a photosensitizer, as an electrostatic linker connecting the nanoparticles and as a probe to investigate the surface composition of the II-VI semiconducting nanoparticles. Different nanoparticles with varying zinc sulfide/manganese sulfide shell ratios are tested with regard to their photocatalytic behavior by crocin bleaching. The results reveal that the shell composition can be a crucial key to optimize the catalytic activity, which can further be important in tuning the reactivity of related systems. Fundamentally, the stepwise multi-component self-assembly in an aqueous solution has been demonstrated to allow the tuning of optical and catalytic properties of core-shell nanoparticles, a general concept that may be widely applicable.

Keywords: core-shell nanoparticles; electrostatic self-assembly; hybrid nanoparticles; polyelectrolytes; porphyrin; photocatalysis



Citation: Wagner, M.; Gröhn, F. The Shell Matters: Self-Organized CdS-ZnS/MnS-Core-Shell—Porphyrin-Polymer Nano-Assemblies for Photocatalysis. *Catalysts* **2022**, *12*, 907. <https://doi.org/10.3390/catal12080907>

Academic Editors: Detlef W. Bahnemann, Ewa Kowalska, Ioannis Konstantinou, Magdalena Janus, Vincenzo Vaiano, Wonyong Choi and Zhi Jiang

Received: 19 July 2022

Accepted: 12 August 2022

Published: 17 August 2022

Publisher's Note: MDPI stays neutral with regard to jurisdictional claims in published maps and institutional affiliations.



Copyright: © 2022 by the authors. Licensee MDPI, Basel, Switzerland. This article is an open access article distributed under the terms and conditions of the Creative Commons Attribution (CC BY) license (<https://creativecommons.org/licenses/by/4.0/>).

1. Introduction

Semiconducting quantum dots have become of great importance as their tunable optical properties are of significance in light-emitting diodes, solar cells, bio labeling, and are of great value in catalysis [1–6]. Currently, it is highly desirable to develop concepts that allow their properties to be further tuned for application in photocatalysis as a route to solar energy conversion or to the decomposition of organic pollutants in wastewater. With this motivation, supramolecularly organized catalysts can be of particular advantage because they can be combined into complex composites that perform various functions in a facile and versatile manner [7–9]. Fine tuning the optical properties of semiconductor nanoparticles can be achieved by varying the size, ligands, and doping [10–14]. The influence of dopants in II-VI semiconductors has been extensively studied for different transition metals, such as manganese(II), nickel(II), silver(I), and copper(I, II) [15–23]. The metal dopant has a strong impact on the semiconductor's photocatalytic properties [24,25]. In particular, the silver(I) dopant enhances the photoluminescence of CdS nanocrystals immensely [21]. By overgrowing the CdS core with wide-bandgap semiconducting layers, the photoluminescence can additionally be increased, as electrons are trapped inside the core [26]. With a bandgap of 3.5 and 3.1 eV, respectively, both ZnS and MnS represent promising wide-bandgap semiconducting materials [27,28].

A great amount of these particles are prepared at high temperature by applying empirically established temperature profiles, and a further assembly has to be performed in further steps after purification. Thus, it is not only highly desirable to create more and more complex and target designed structures with such core-shell quantum dots, but also

to establish routes for an energy-effective and environment-friendly synthesis, preferably in water and at room temperature. Recently, we have shown for the first time that ternary structures can be obtained by a combination of electrostatic nanotemplating in poly(acrylic acid) and self-assembly in an aqueous solution [29]. This attempt is comparable to the self-assembly of purely inorganic structures [30]. Yet, the wide range of polymers allow these systems to be adjusted by multiple interactions. These possibilities to target design the optic and catalytic properties of hybrid core-shell quantum dots, and thereby also the generality of this concept, are yet to be exploited [31–34].

Herein, we investigate the possibility to build core-shell semiconductor quantum dots inside a polyelectrolyte and connect them with a porphyrin photosensitizer directly in aqueous solution. The goal is an enhancing photocatalytic activity of silver-doped CdS covered with a ZnS/MnS shell of different compositions combined with 5,10,15,20-tetrakis(4-trimethyl-ammoniohenyl) porphyrin (TAPP) as a photosensitizer, increasing the spectral range of poorly absorbing inorganic nanoparticles. Poly(acrylic acid) (PAA) stabilizes the core-shell nanoparticles in aqueous solution and enables their further interconnection. In addition to its role as a photosensitizer, TAPP serves as an electrostatic linker, connecting the negatively charged CdS-Zn_xMn_{1-x}S nanoparticles into larger supramolecular structures in aqueous solution (Figure 1). The two metals, manganese and zinc, are used to form a shell with mixed ratios of MnS and ZnS with a variety of compositions—far from the typical dopant concentration in nanoparticles. The structures were analyzed by transmission electron microscopy (TEM), dynamic light scattering (DLS), and absorption and emission spectroscopy. This system was tested with regard to its photocatalytic activity in dependence on the shell composition, that is, the ratio of ZnTAPP to MnTAPP.

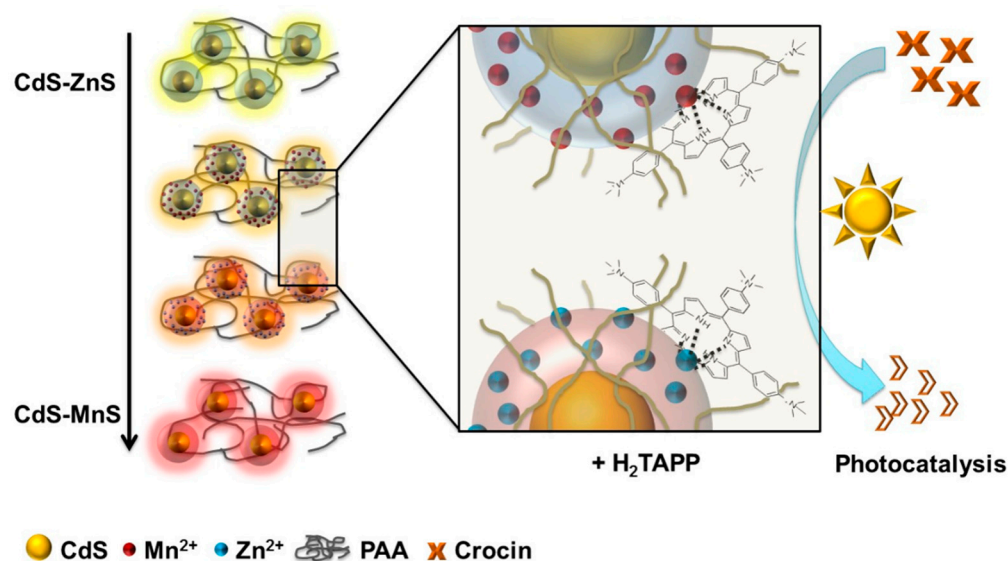


Figure 1. Scheme of catalytically active assemblies with tunable spectral properties: fluorescent color change in dependence on increasing manganese content in the shell and interaction of TAPP with the inorganic nanoparticles.

2. Results

Synthesis of the core-shell nanoparticles was performed in aqueous medium at room temperature in the presence of poly(acrylic acid), known as “electrostatic nanotemplating” [35–39]. Here, first the anionic polyelectrolyte was loaded with cadmium ions and by the addition of sulfide, CdS nanoparticles formed inside the polyelectrolyte template. The surrounding ZnS/MnS shell was built accordingly (see SI). After the synthesis of the core nanoparticles, the size of CdS was determined from UV/vis spectroscopy using the Henglein equation [40]. The mean size of the core was determined to be 2.0 nm, which is valid for all synthesized CdS-Zn_xMn_{1-x}S nanoparticles herein. The diameter of the CdS-ZnS

core-shell nanocrystals was then determined via transmission electron microscopy (TEM), which revealed nanoparticles with an average size of 3.6 nm (Figure 2a). Hence, the layer thickness of ZnS covering the CdS core was about 0.8 nm. The HR-TEM revealed a lattice distance of 0.33 nm, which fit well into the wurtzite lattice of the metal sulfide compounds. This specific distance was determined for the CdS-Zn_{0.5}Mn_{0.5}S and CdS-MnS (see SI) with only slight deviations. TEM of CdS-Zn_{0.05}Mn_{0.95}S (see Supplementary Figure S2) revealed a size of about 4.1 nm, leading to a MnS layer thickness of approximately 1 nm, which aligns with the previous results as the atomic radius of Mn²⁺ is larger than that of Zn²⁺, leading to a slightly thicker layer with a higher contrast in the TEM. Dynamic light scattering (DLS) was used to investigate the sizes of the CdS-ZnS nanoparticle–PAA assemblies before and after combination with the cationic TAPP directly in aqueous solution (Figure 2b). To detect a possible key to the stability and size tuning of the hybrid particles, the charge ratio l —that is, the molar concentration of the positively-charged amines of TAPP divided by the molar concentration of the negatively-charged acid groups of PAA—was varied. Assemblies with a narrow size distribution and a hydrodynamic radius from $R_H = 38$ nm (distribution width $\sigma = 0.06$) for $l = 0.06$ to $R_H = 58$ nm (distribution width $\sigma = 0.2$) for $l = 0.250$ were found. The size increase with increasing amount of porphyrin is due to the integration of higher amounts of porphyrin into the structure favored by electrostatic interactions of the negatively-charged PAA and the positively-charged porphyrin. From static light scattering (SLS), the radius of gyration (R_G) was obtained, such that the shape characteristic was the R_G/R_H ratio, which gives an indication of the assembly structure. The ratio of $R_G/R_H = 1.3$ could be found for all samples, indicating the formation of slightly elongated structures. In contrast, above $l = 0.38$ the resulting hybrid nanoparticles were polydispersed in size and started to sediment fast at a charge ratio of $l = 0.5$. Due to the small amounts of larger aggregates, filtration of the solution was crucial.

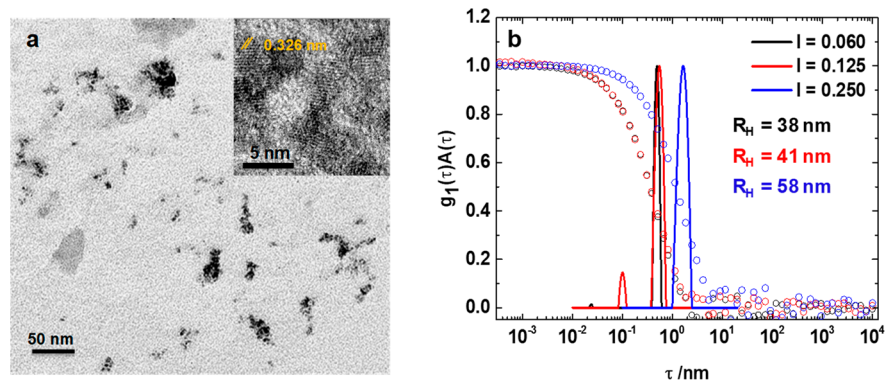


Figure 2. (a) TEM and HR-TEM image of PAA-capped CdS-ZnS nanoparticles, (b) dynamic light scattering: electric field autocorrelation function (dots) and distribution of relaxation times (lines) of CdS-ZnS-TAPP aggregates with charge ratio 0.060 (black), 0.125 (red) and 0.250 (blue).

Absorption and fluorescence spectroscopy were used to investigate the optical properties, providing further information on the lattice morphology at the core-shell interface. A stepwise increase in the Mn(II) content in the shell led to a red shift in the absorption and emission spectrum of the nanoparticles (Figure 3a,b). This result may be due to lattice mismatches or strained shell lattices in the CdS-MnS interface, which can further explain the abrupt decrease in photoluminescence occurring at a Mn(II) content of 95% [41–43].

TAPP can serve as a probe to inspect the atomic composition on the surface of the semiconducting nanoparticles. The addition of TAPP to CdS-Zn_xMn_{1-x}S gives rise to a ZnTAPP and MnTAPP sitting atop the complex at varying ratios with respect to the Zn-MnS shell composition. The respective Soret-band of ZnTAPP can be found at 435 nm (Figure 3c, black curve), which is far from its in-plane analogue and cannot be explained by a simple bathochromic shift due to incorporation into the polymer matrix [44]. The Soret band of Mn(II)TAPP is located at 461 nm (Figure 3c, red curve). Since Mn(II) is too large to fit into

the pyrrol ring cavity, it preferentially forms sitting atop complexes with porphyrins [45,46].

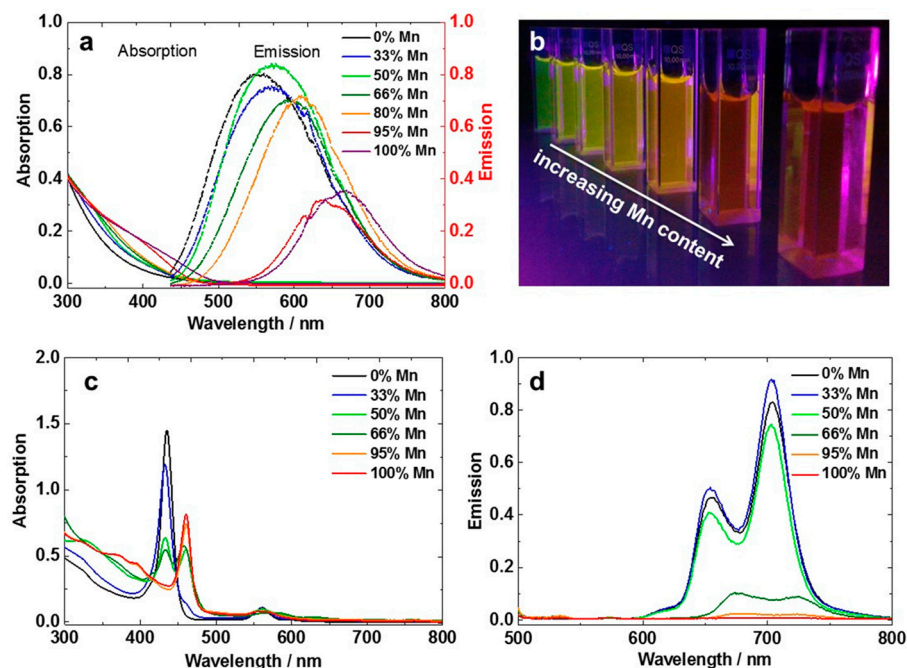


Figure 3. (a) Absorption and emission spectra of CdS-Zn_xMn_{1-x} with different Zn:Mn ratios in the shell (excited at 300 nm), (b) picture of fluorescing CdS-Zn_xMn_{1-x} nanoparticles, (c) absorption and (d) emission spectra of CdS-Zn_xMn_{1-x}-TAPP (excited at 447 nm).

The formation of MnTAPP and ZnTAPP can be observed instantly after the addition of TAPP to the pure CdS-ZnS and CdS-MnS, respectively. For mixed shells, the formation of ZnTAPP occurs shortly after the addition, whereas the formation of MnTAPP is completed after 30 min. An incomplete surface coverage with the shell would be seen here as well. The TAPP complexes with CdS particles show a characteristic absorption band at 447 nm, which is also sensitive to the loading of porphyrin (Supplementary Figure S5). The emission of the porphyrin attached to the surface of the nanocrystals was completely quenched for high manganese contents excited at the isosbestic point at 447 nm. A strong decrease in the fluorescence of TAPP is found from a 1:1 (Mn:Zn) shell to the 2:1 (Mn:Zn) shell, which likely indicates a change in the shell lattice between these two ratios.

Since optical properties are connected to photocatalytic activity, it is now of high interest to investigate the reactivity in photocatalysis by studying the light-induced degradation of crocin as a model reaction. Crocin is chosen as an unsaturated carbon backbone in combination with its glucose moieties. The latter provides a high concentration of the dye, to demonstrate that the catalysts perform well at high concentrations of, e.g., pollutant, and the hybrid aggregate is not influenced. The mechanism of degradation occurs via reactive oxygen species, breaking the conjugation in the carbon backbone [47]. A loading ratio of 0.06 was chosen in order to use only low amounts of porphyrin. Results are given in Figure 4. All CdS-Zn_xMn_{1-x}S-TAPP aggregates show reactivity toward crocin. The catalytic activity was also judged based on the decomposition after a one-hour reaction time, plotted versus the shell composition in Figure 4d.

Starting with CdS-ZnS-TAPP, the degree of degradation increases with an increasing amount of manganese. At a manganese content of 33 and 50%, the highest decomposition rates are reached and accordingly decrease with the increasing manganese ratio, leading to the lowest degradation rate for CdS-Zn_{0.05}Mn_{0.95}S. With CdS-MnS-TAPP, the reaction velocity increases again, which likely is a result of a more homogeneous MnS surface. This can also be seen in the emission spectrum of CdS-Zn_{0.05}Mn_{0.95}S and CdS-MnS (Figure 2, orange curve), where CdS-MnS provides higher photoluminescence than CdS-Zn_{0.05}Mn_{0.95}S.

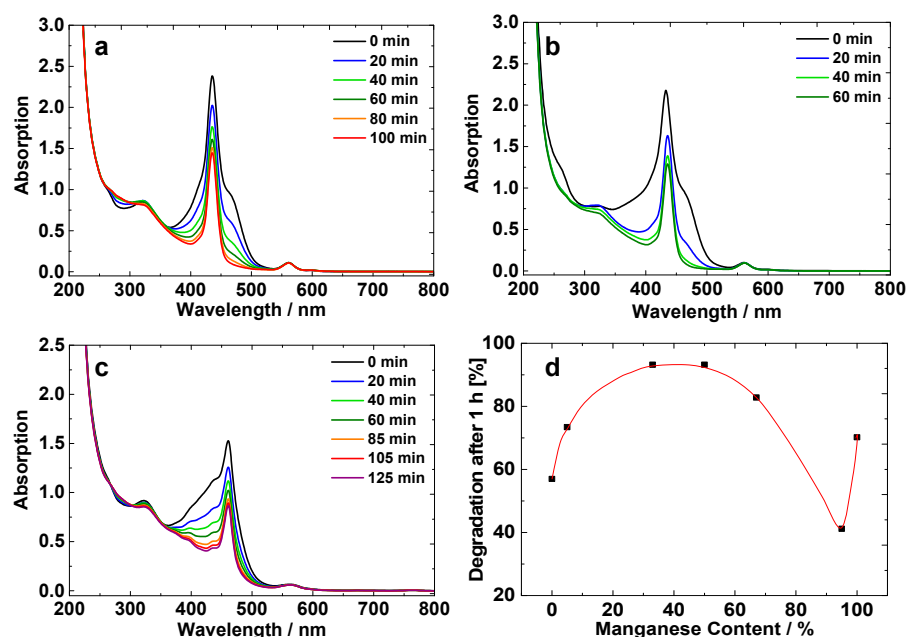


Figure 4. Photocatalytic model reaction of crocin with (a) CdS-Zn_{0.95}Mn_{0.05}-TAPP, (b) CdS-Zn_{0.33}Mn_{0.67}-TAPP, (c) CdS-Zn_{0.05}Mn_{0.95}-TAPP and (d) dependence of degradation rate on the manganese content in the shell.

3. Discussion

The photocatalytic behavior displays that the activity cannot only benefit from pristine CdS-ZnS or CdS-MnS nanoparticles or shell compositions close to the pristine materials since the high band gaps of MnS and ZnS prevent electron transfer. This can be seen in the negligible catalytic performances of the pristine particles (Supplementary Figure S3). The CdS core and TAPP cannot provide a significant degradation when tested separately [29]. However, it is possible to achieve decent catalytic activity for the CdS-MnS core-shell structures for other catalysis processes [48]. By changing the composition to more equal amounts of ZnS and MnS, the catalytic activity is affected drastically, indicating a beneficial contribution of the inorganic shell. Apparently, the mixture of these gives access to the core, likely with trap states in the core-shell interface. Hence, an electron transfer mechanism including the shell as the medium or direct target takes place. In this, manganese in the shell can serve as an electron donor for ZnTAPP/MnTAPP, leading to the highest catalytic activity for CdS-Zn_{0.66}Mn_{0.34}S-TAPP and CdS-Zn_{0.5}Mn_{0.5}S, where higher contents of ZnTAPP can be found on the surface [49,50]. At amounts above 50%, manganese states likely are replaced by continuous bands of larger manganese sulfide clusters inside the shell, which cannot enhance the electron transfer anymore. Thus, an optimum composition of CdS-MnS core-shell particles in ternary assemblies for the photocatalytic model reaction in water has been identified.

Recently, related self-assembled systems have successfully demonstrated their catalytic ability, but those consisted of fewer components [9,29]. Herein, the multicomponent structure target designed for a certain function demonstrates that further complexity can simply be generated by self-assembly in water, representing a key for expanding the scope of other catalytic materials.

4. Materials and Methods

Chemicals. Cadmium nitrate tetrahydrate (99.999% trace metals basis), zinc chloride (99.99% trace metals basis), manganese chloride tetrahydrate, sodium sulfide nonahydrate ($\geq 98.0\%$), silver nitrate ($\geq 99.0\%$) and poly(acrylic acid) (Average M_W 100,000 g mol⁻¹) (PAA100k) were purchased from Sigma Aldrich (Schnelldorf, Germany). 5,10,15,20-Tetrakis

(4-trimethylammonio-phenyl) porphyrin tetrachloride (H₂TAPP) was purchased from Fluka (Charlotte, NC, USA).

In all experiments, deionized water was used, which was filtered through a 0.20 µm hydrophilic filter purchased from Millex (Merck, Darmstadt, Germany).

Sample preparation. The synthesis of Ag-doped CdS-Zn_xMn_{1-x}S core-shell nanoparticles were achieved in a two-step approach. First the CdS core was prepared via precipitating CdNO₃ (2.9×10^{-4} mol L⁻¹) and AgNO₃ (4.4×10^{-6} mol/L) with Na₂S (4.2×10^{-4} mol L⁻¹) in presence of PAA100k (c(Monomer) = 3.4×10^{-4} mol L⁻¹) in deionized water at pH = 7. In a second step, ZnCl₂ and MnCl₂ were added in their respective ratios keeping the overall concentration of the additional cations constant at 2.2×10^{-4} mol L⁻¹. Subsequently, Na₂S (3.0×10^{-4} mol L⁻¹) was injected to form the shells and the pH was adjusted to 10.5 using 1 M NaOH. An increasing concentration of Mn(II) in the shell lead to darker yellow solutions. The growth of the NPs was observed with a UV lamp resulting in longer growth times for higher Mn content in the shell. The growth of CdS-MnS was completed after 5 h.

To the readily formed nanoparticles, a solution of 5,10,15,20-tetrakis(4-trimethylammonio-phenyl) porphyrin (H₂TAPP) in deionized water was added and the sample was filtered with a 0.450 µm PTFE filter. The charge ratio l (-NMe₃⁺ / -COO⁻) was set to 0.060 (c(H₂TAPP) = 5.1×10^{-5} mol L⁻¹), 0.125 (c(H₂TAPP) = 1.1×10^{-4} mol L⁻¹) and 0.250 (c(H₂TAPP) = 2.1×10^{-5} mol L⁻¹).

Characterization techniques. For the light scattering experiment, a CGS 3 goniometer (ALV, Langen, Germany) with a 22 mW laser providing a wavelength of 632.8 nm and an ALV 5000 correlator with 320 channels were used. During the measurement, the angles between 30 and 150° were covered in 10° steps. Data analysis of dynamic light scattering was performed via transformation of the autocorrelation function of the scattered light into the autocorrelation function of the electric field using Siegert equation. The inverse Laplace transformation was carried out with the program CONTIN.

UV/vis measurements were taken out with a Shimadzu UV-spectrometer (UV-1800) (Shimadzu Germany, Duisburg, Germany). Quartz cuvettes with a pathlength of 1 cm and 1 mm purchased from Hellma/Müllheim were used, respectively.

Fluorescence measurements were performed with a Horiba Yvon Jobin fluorescence spectrometer (Horiba, Oberursel, Germany) using a slit width of 3 nm and an integration time of 0.1 s.

The transmission electron microscopy (TEM) images were performed with a Zeiss EM 912 microscope, operated at 80 kV at magnifications ranging from 20,000 to 250,000. The specimens were prepared by depositing 5 µL of the sample solution onto carbon-coated copper grids, 300 mesh, and air-drying the grids. The sizes of the particles were determined using the freely available software ImageJ (Version 1.51h, open source).

Photodegradation of crocin. The photocatalytic decomposition of crocin (purchased from Sigma Aldrich) was performed in aqueous medium using 3 mL of the initial catalyst stock solution (at pH 10.5). To this solution, 60 µL of a 3.3×10^{-3} mol L⁻¹ crocin stock solution were added. The irradiation was taken out with a 500 W lamp and the reaction process was detected every 20 min for the first hour.

5. Conclusions

In conclusion, a new type of powerful supramolecular photocatalytic system in water was built from a core-shell nanoparticle assembly with tunable optical properties prepared in water with mediating anionic poly(acrylic acid) in combination with a tetravalent cationic porphyrin. Thereby, the nanoparticle shell determined the catalytic activity. A shell stoichiometry Zn_{0.66}Mn_{0.34}S led to a strong increase in the catalytic activity of the CdS-Zn_xMn_{1-x}S-TAPP assemblies in contrast to a pure ZnS or MnS shell. This can likely be attributed to active manganese states in the shell allowing electron transport through the shell. The photocatalytic activity of CdS-ZnS and CdS-MnS was lower and identical, which is due to the high bandgap of the shell sulfides leading to a screening of the CdS core

and TAPP. Further, the shell composition was investigated via UV/vis spectroscopy by taking advantage of porphyrin as a sensitive probe for surface atoms. The electrostatic self-assembly of the PAA stabilized inorganic 3.6 nm nanoparticles with the cationic porphyrin led to their interconnection and to well-defined assemblies with a tunable size in the range of $38 \leq R_H \leq 58$ nm, which were stable in aqueous solution.

Overall, synthesis in water, which avoids toxic precursors and solvents, combined with multi-component modular self-assembly—again in water—offers a versatile and tunable concept for a targeted structure design. This may have an impact on solar energy conversion. The beneficial effect of co-dopants in core-shell nanostructures on catalytic behavior may be extended to related systems, including wide bandgap semiconductors such as ZnO and TiO₂. The polymeric basis can allow such composites to be deposited onto metallic or semiconducting surfaces as a functional polymer film.

Supplementary Materials: The following supporting information can be downloaded at: <https://www.mdpi.com/article/10.3390/catal12080907/s1>, Figure S1: Absorption and emission spectra of TAPP, Figure S2: TEM images of CdS–ZnS core–shell nanoparticles, Figure S3: Absorption spectrum of crocin and time dependent photo-bleaching reaction of crocin with CdS–Zn_xMn_{1-x}S–TAPP aggregates including references without TAPP, Figure S4: Absorption spectra of crocin with CdS–Core-shell zinc manganese mixtures, Figure S5: Absorption spectra of TAPP binding to a CdS particle in dependence of TAPP concentration.

Author Contributions: Conceptualization, methodology, and writing: M.W. and F.G.; experiments: M.W.; supervision and funding acquisition: F.G. All authors have read and agreed to the published version of the manuscript.

Funding: This research was funded by Deutsche Forschungsgemeinschaft (DFG, GR 2701/6-1), Solar Technologies go Hybrid (SolTech).

Data Availability Statement: Data can be found in the Electronic Supplementary Materials and can be requested from the authors.

Conflicts of Interest: The authors declare no conflict of interest.

References

1. Kim, S.; Fisher, B.; Eisler, H.-J.; Bawendi, M. Type-II quantum dots: CdTe/CdSe(core/shell) and CdSe/ZnTe(core/shell) heterostructures. *J. Am. Chem. Soc.* **2003**, *125*, 11466–11467. [[CrossRef](#)]
2. Lee, J.; Sundar, V.C.; Heine, J.R.; Bawendi, M.G.; Jensen, K.F. Full Color Emission from II-VI Semiconductor Quantum Dot-Polymer Composites. *Adv. Mater.* **2000**, *12*, 1102–1105. [[CrossRef](#)]
3. Robel, I.; Subramanian, V.; Kuno, M.; Kamat, P.V. Quantum dot solar cells. harvesting light energy with CdSe nanocrystals molecularly linked to mesoscopic TiO₂ films. *J. Am. Chem. Soc.* **2006**, *128*, 2385–2393. [[CrossRef](#)]
4. Lee, Y.-L.; Lo, Y.-S. Highly Efficient Quantum-Dot-Sensitized Solar Cell Based on Co-Sensitization of CdS/CdSe. *Adv. Funct. Mater.* **2009**, *19*, 604–609. [[CrossRef](#)]
5. Dyadyusha, L.; Yin, H.; Jaiswal, S.; Brown, T.; Baumberg, J.J.; Booy, F.P.; Melvin, T. Quenching of CdSe quantum dot emission, a new approach for biosensing. *Chem. Commun.* **2005**, *25*, 3201–3203. [[CrossRef](#)] [[PubMed](#)]
6. Medintz, I.L.; Clapp, A.R.; Mattoussi, H.; Goldman, E.R.; Fisher, B.; Mauro, J.M. Self-assembled nanoscale biosensors based on quantum dot FRET donors. *Nat. Mater.* **2003**, *2*, 630–638. [[CrossRef](#)] [[PubMed](#)]
7. Krieger, A.; Zika, A.; Gröhn, F. Functional Nano-Objects by Electrostatic Self-Assembly: Structure, Switching, and Photocatalysis. *Front. Chem.* **2021**, *9*, 779360. [[CrossRef](#)] [[PubMed](#)]
8. Bernhardt, S.; Düring, J.; Haschke, S.; Barr, M.K.S.; Stiegler, L.; Schühle, P.; Bachmann, J.; Hirsch, A.; Gröhn, F. Tunable Photocatalytic Activity of PEO-Stabilized ZnO–Polyoxometalate Nanostructures in Aqueous Solution. *Adv. Mater. Interfaces* **2021**, *8*, 2002130. [[CrossRef](#)]
9. Wagner, M.; Waleska, N.; Gröhn, F. Hybrid Organic–Platinum Nanoparticles for Hydrogenation Reactions. *ACS Appl. Nano Mater.* **2021**, *4*, 4329–4334. [[CrossRef](#)]
10. Wang, Y.; Herron, N. Nanometer-sized semiconductor clusters: Materials synthesis, quantum size effects, and photophysical properties. *J. Phys. Chem.* **1991**, *95*, 525–532. [[CrossRef](#)]
11. Alivisatos, A.P. Semiconductor Clusters, Nanocrystals, and Quantum Dots. *Science* **1996**, *271*, 933–937. [[CrossRef](#)]
12. Kalyuzhny, G.; Murray, R.W. Ligand effects on optical properties of CdSe nanocrystals. *J. Phys. Chem. B* **2005**, *109*, 7012–7021. [[CrossRef](#)] [[PubMed](#)]

13. Comparelli, R.; Zezza, F.; Striccoli, M.; Curri, M.L.; Tommasi, R.; Agostiano, A. Improved optical properties of CdS quantum dots by ligand exchange. *Mater. Sci. Eng. C* **2003**, *23*, 1083–1086. [[CrossRef](#)]
14. Yu, W.W.; Wang, Y.A.; Peng, X. Formation and Stability of Size-, Shape-, and Structure-Controlled CdTe Nanocrystals: Ligand Effects on Monomers and Nanocrystals. *Chem. Mater.* **2003**, *15*, 4300–4308. [[CrossRef](#)]
15. Dandia, A.; Parewa, V.; Rathore, K.S. Synthesis and characterization of CdS and Mn doped CdS nanoparticles and their catalytic application for chemoselective synthesis of benzimidazoles and benzothiazoles in aqueous medium. *Catal. Commun.* **2012**, *28*, 90–94. [[CrossRef](#)]
16. Liu, S.-M.; Liu, F.-Q.; Guo, H.-Q.; Zhang, Z.-H.; Wang, Z.-G. Surface states induced photoluminescence from Mn²⁺ doped CdS nanoparticles. *Solid State Commun.* **2000**, *115*, 615–618. [[CrossRef](#)]
17. Thambidurai, M.; Muthukumarasamy, N.; Agilan, S.; Sabari Arul, N.; Murugan, N.; Balasundaraprabhu, R. Structural and optical characterization of Ni-doped CdS quantum dots. *J. Mater. Sci.* **2011**, *46*, 3200–3206. [[CrossRef](#)]
18. Henglein, A. Photo-Degradation and Fluorescence of Colloidal-Cadmium Sulfide in Aqueous Solution. *Ber. Bunsenges. Phys. Chem.* **1982**, *86*, 301–305. [[CrossRef](#)]
19. Zeng, R.; Sun, Z.; Cao, S.; Shen, R.; Liu, Z.; Xiong, Y.; Long, J.; Zheng, J.; Zhao, Y.; Shen, Y.; et al. Facile synthesis of Ag-doped ZnCdS nanocrystals and transformation into Ag-doped ZnCdS_{Se} nanocrystals with Se treatment. *RSC Adv.* **2015**, *5*, 1083–1090. [[CrossRef](#)]
20. Tang, A.; Yi, L.; Han, W.; Teng, F.; Wang, Y.; Hou, Y.; Gao, M. Synthesis, optical properties, and superlattice structure of Cu(I)-doped CdS nanocrystals. *Appl. Phys. Lett.* **2010**, *97*, 33112. [[CrossRef](#)]
21. Vaiano, V.; Matarangolo, M.; Murcia, J.J.; Rojas, H.; Navío, J.A.; Hidalgo, M.C. Enhanced photocatalytic removal of phenol from aqueous solutions using ZnO modified with Ag. *Appl. Catal. B Environ.* **2018**, *225*, 197–206. [[CrossRef](#)]
22. Vaiano, V.; Iervolino, G.; Rizzo, L. Cu-doped ZnO as efficient photocatalyst for the oxidation of arsenite to arsenate under visible light. *Appl. Catal. B Environ.* **2018**, *238*, 471–479. [[CrossRef](#)]
23. Karamoschos, N.; Bairamis, F.; Andrikopoulos, K.S.; Konstantinou, I.; Tasis, D. Metal-doped CdS/MoS₂ heterojunctions for photocatalytic degradation of organic pollutant. *Mater. Sci. Semicond. Processing* **2022**, *144*, 106600. [[CrossRef](#)]
24. Ullah, R.; Dutta, J. Photocatalytic degradation of organic dyes with manganese-doped ZnO nanoparticles. *J. Hazard. Mater.* **2008**, *156*, 194–200. [[CrossRef](#)]
25. Hamal, D.B.; Klabunde, K.J. Synthesis, characterization, and visible light activity of new nanoparticle photocatalysts based on silver, carbon, and sulfur-doped TiO₂. *J. Colloid Interface Sci.* **2007**, *311*, 514–522. [[CrossRef](#)]
26. Talapin, D.V.; Mekis, I.; Götzinger, S.; Kornowski, A.; Benson, O.; Weller, H. CdSe/CdS/ZnS and CdSe/ZnSe/ZnS Core–Shell–Shell Nanocrystals. *J. Phys. Chem. B* **2004**, *108*, 18826–18831. [[CrossRef](#)]
27. Steckel, J.S.; Zimmer, J.P.; Coe-Sullivan, S.; Stott, N.E.; Bulović, V.; Bawendi, M.G. Blue Luminescence from (CdS)ZnS Core–Shell Nanocrystals. *Angew. Chem.* **2004**, *116*, 2206–2210. [[CrossRef](#)]
28. Tsuji, I.; Kato, H.; Kudo, A. Visible-Light-Induced H₂ Evolution from an Aqueous Solution Containing Sulfide and Sulfite over a ZnS-CuInS₂-AgInS₂ Solid-Solution Photocatalyst. *Angew. Chem.* **2005**, *117*, 3631–3634. [[CrossRef](#)]
29. Wagner, M.; Strassert, C.A.; Gröhn, F. Hierarchical electrostatic nanotemplating and assembly of electron-transferring hybrid nanostructures: CdS-polymer-porphyrin particles. *Nanoscale* **2022**. [[CrossRef](#)]
30. Fan, H.; Maheshwari, V. Controlled Element Specific Nanoscale Domains by Self-Assembly for High Performance Bifunctional Alkaline Water Splitting Catalyst. *Adv. Funct. Mater.* **2021**, *31*, 2106149. [[CrossRef](#)]
31. Lokhande, C.D.; Ennaoui, A.; Patil, P.S.; Giersig, M.; Muller, M.; Diesner, K.; Tributsch, H. Process and characterisation of chemical bath deposited manganese sulphide (MnS) thin films. *Thin Solid Film.* **1998**, *330*, 70–75. [[CrossRef](#)]
32. Walter, M.G.; Wamser, C.C.; Ruwitch, J.; Zhao, Y.; Braden, D.; Stevens, M.; Denman, A.; Pi, R.; Rudine, A.; Pessiki, P.J. Syntheses and optoelectronic properties of amino/carboxyphenylporphyrins for potential use in dye-sensitized TiO₂ solar cells. *J. Porphyr. Phthalocyanines* **2007**, *11*, 601–612. [[CrossRef](#)]
33. Ruthard, C.; Schmidt, M.; Gröhn, F. Porphyrin-polymer networks, worms, and nanorods: pH-triggerable hierarchical self-assembly. *Macromol. Rapid Commun.* **2011**, *32*, 706–711. [[CrossRef](#)] [[PubMed](#)]
34. Frühbeißer, S.; Gröhn, F. Catalytic activity of macroion-porphyrin nanoassemblies. *J. Am. Chem. Soc.* **2012**, *134*, 14267–14270. [[CrossRef](#)] [[PubMed](#)]
35. Antonietti, M.; Gröhn, F.; Hartmann, J.; Bronstein, L. Nonclassical Shapes of Noble-Metal Colloids by Synthesis in Microgel Nanoreactors. *Angew. Chem. Int. Ed. Engl.* **1997**, *36*, 2080–2083. [[CrossRef](#)]
36. Gröhn, F.; Bauer, B.J.; Akpalu, Y.A.; Jackson, C.L.; Amis, E.J. Dendrimer Templates for the Formation of Gold Nanoclusters. *Macromolecules* **2000**, *33*, 6042–6050. [[CrossRef](#)]
37. Zhang, J.; Xu, S.; Kumacheva, E. Polymer microgels: Reactors for semiconductor, metal, and magnetic nanoparticles. *J. Am. Chem. Soc.* **2004**, *126*, 7908–7914. [[CrossRef](#)]
38. Xu, Y.; Yuan, J.; Fang, B.; Drechsler, M.; Müllner, M.; Bolisetty, S.; Ballauff, M.; Müller, A.H.E. Hybrids of Magnetic Nanoparticles with Double-Hydrophilic Core/Shell Cylindrical Polymer Brushes and Their Alignment in a Magnetic Field. *Adv. Funct. Mater.* **2010**, *20*, 4182–4189. [[CrossRef](#)]
39. Düring, J.; Hölzer, A.; Kolb, U.; Branscheid, R.; Gröhn, F. Supramolecular Organic–Inorganic Hybrid Assemblies with Tunable Particle Size: Interplay of Three Noncovalent Interactions. *Angew. Chem. Int. Ed.* **2013**, *52*, 8742–8745. [[CrossRef](#)]

40. Spanhel, L.; Haase, M.; Weller, H.; Henglein, A. Photochemistry of colloidal semiconductors. Surface modification and stability of strong luminescing CdS particles. *J. Am. Chem. Soc.* **1987**, *109*, 5649. [[CrossRef](#)]
41. Brus, L.E. A simple model for the ionization potential, electron affinity, and aqueous redox potentials of small semiconductor crystallites. *J. Chem. Phys.* **1983**, *79*, 5566. [[CrossRef](#)]
42. Zuo, T.; Sun, Z.; Zhao, Y.; Jiang, X.; Gao, X. The big red shift of photoluminescence of Mn dopants in strained CdS: A case study of Mn-doped MnS-CdS heteronanostructures. *J. Am. Chem. Soc.* **2010**, *132*, 6618–6619. [[CrossRef](#)] [[PubMed](#)]
43. Davis, A.H.; Hofman, E.; Chen, K.; Li, Z.-J.; Khammang, A.; Zamani, H.; Franck, J.M.; Maye, M.M.; Meulenberg, R.W.; Zheng, W. Exciton Energy Shifts and Tunable Dopant Emission in Manganese-Doped Two-Dimensional CdS/ZnS Core/Shell Nanoplatelets. *Chem. Mater.* **2019**, *31*, 2516–2523. [[CrossRef](#)]
44. Yang, Y.; Chen, O.; Angerhofer, A.; Cao, Y.C. Radial-Position-Controlled Doping of CdS/ZnS Core/Shell Nanocrystals: Surface Effects and Position-Dependent Properties. *Chem. Eur. J.* **2009**, *15*, 3186–3197. [[CrossRef](#)] [[PubMed](#)]
45. Yuanqian, L.; Jingmei, H.; Jingguo, Y.; Bo, Z.; Yuanqing, H. Multi-component analysis by flow injection-diode array detection-spectrophotometry using partial least squares calibration model for simultaneous determination of zinc, cadmium and lead. *Anal. Chim. Acta* **2002**, *461*, 181–188. [[CrossRef](#)]
46. Inada, Y.; Nakano, Y.; Inamo, M.; Nomura, M.; Funahashi, S. Structural characterization and formation mechanism of sitting-atop (SAT) complexes of 5, 10, 15, 20-tetraphenylporphyrin with divalent metal ions. Structure of the Cu(II)-SAT complex as determined by fluorescent extended X-ray absorption fine structure. *Inorg. Chem.* **2000**, *39*, 4793–4801. [[CrossRef](#)]
47. Semitsoglou-Tsiapou, S.; Meador, T.B.; Peng, B.; Aluwihare, L. Photochemical (UV-vis/H₂O₂) degradation of carotenoids: Kinetics and molecular end products. *Chemosphere* **2022**, *286*, 131697. [[CrossRef](#)]
48. Fang, X.; Cui, L.; Pu, T.; Song, J.; Zhang, X. Core-shell CdS@MnS nanorods as highly efficient photocatalysts for visible light driven hydrogen evolution. *Appl. Surf. Sci.* **2018**, *457*, 863–869. [[CrossRef](#)]
49. Begum, R.; Chattopadhyay, A. Redox-Tuned Three-Color Emission in Double (Mn and Cu) Doped Zinc Sulfide Quantum Dots. *J. Phys. Chem. Lett.* **2014**, *5*, 126–130. [[CrossRef](#)]
50. Sheng, P.; Li, W.; Tong, X.; Wang, X.; Cai, Q. Development of a high performance hollow CuInSe₂ nanospheres-based photoelectrochemical cell for hydrogen evolution. *J. Mater. Chem. A* **2014**, *2*, 18974–18987. [[CrossRef](#)]